Journal of Solid State Chemistry 186 (2012) 171–176

Contents lists available at SciVerse ScienceDirect

Journal of Solid State Chemistry

journal homepage: www.elsevier.com/locate/jssc

Spectroscopic studies of sulfite-based polyoxometalates at high temperature and high pressure

Raul Quesada Cabrera [a], Steven Firth [a], Christopher S. Blackman [a], De-Liang Long [b], Leroy Cronin [b,**], Paul F. McMillan [a,*]

[a] Department of Chemistry and Materials Chemistry Centre, Christopher Ingold Laboratories, University College London, 20 Gordon St., London WC1H 0AJ, United Kingdom
[b] WestChem, School of Chemistry, The University of Glasgow, Glasgow G12 8QQ, United Kingdom

ARTICLE INFO

Article history:
Received 10 August 2011
Received in revised form
3 December 2011
Accepted 4 December 2011
Available online 13 December 2011

Keywords:
Polyoxometalates
Spectroscopy
Bronze-like species
High temperature
High pressure
Thermochromic properties

ABSTRACT

Structural changes occurring within non-conventional Dawson-type $[\alpha/\beta\text{-}Mo_{18}O_{54}(SO_3)_2]^{4-}$ polyanions in the form of tetrapentylammonium salts were studied by a combination of IR, Raman and visible spectroscopy at high temperature and high pressure. Evidence of the formation of bronze-type materials above 400 K and also upon pressurization to 8 GPa is presented. This conclusion is suggested to be a general result for polyoxometalate compounds subjected to extreme conditions and it opens opportunities for the design of new materials with interesting optical and electronic properties.

1. Introduction

Polyoxometalates (POMs) form a large family of heteropolyanions based on octahedrally bonded metal-oxygen units MO_x (M=W, Mo, V, Nb, etc.) that often contain anions such as SO_4^{2-}, PO_4^{3-}, etc. included within the cages [1]. These compounds are interesting for their electronic and optical properties and they are used in a wide range of applications, such as photocatalysis, sensors, switching devices, etc. An important aspect in the investigation of these materials is the study of their performance and stability at non-ambient conditions. These studies have mainly focused on relatively small clusters, Keggin-type $[M_{12}O_{40}]^{n-}$ POMs. Reports on the stability and behavior of larger Wells–Dawson $[M_{18}O_{54}]^{n-}$ clusters at high temperature are scarce in the literature. Surprisingly, there are only a few studies involving POMs at high pressure so far, despite the potential of POM precursors in the synthesis of new nanoscale materials with interesting electronic/magnetic properties via high-pressure methods. Cubic Na_xMoO_3 bronzes have been synthesized in large-volume high-pressure devices at ~6 GPa from mixtures of metallic Mo and oxide precursors [2] and also in diamond anvil cell from $Na_2MoO_4 \cdot 2H_2O$ at 1000–1273 K and 5–8 GPa [3]. Recently, NH_4^+-containing tungsten bronzes have been synthesized at high pressure (10 GPa) and temperature (~1000 K) from a Keggin POM precursor using a large-volume press [4]. This new material exhibited the highest transition temperature reported among this family of compounds, with superconductivity extending up to 5.2 K. We recently reported the first high-pressure study of a Wells–Dawson structure in a diamond anvil cell (DAC) [5], showing the formation of tungsten-based bronze-type species at high pressure.

The materials studied here are non-conventional Dawson-type POM structures, containing two pyramidal SO_3^{2-} groups located inside each metal oxide cage. Two structural types, with formula $(C_{20}H_{44}N)_4$-$[Mo_{18}O_{54}(SO_3)_2]CH_3CN$, are known [6,7], with internal oxygen atoms arranged either in eclipsed (α) or staggered (β) configurations (Fig. 1). These yellow–orange compounds show reversible thermochromism within the range between 77 and 400 K. Recently, we reported a vibrational spectroscopy study at low temperature [8] that contributed to explain this interesting process in terms of interaction between the sulfur atoms. This reversible reduction phenomena has also been observed to occur during thermal activation on a gold surface [9]. At the same time, heating above ~400 K induces an irreversible color change to green/blue due to the VI/V reduction of the Mo ions in the cluster. The latter transformation normally occurs without large structural changes in the cluster and it is a common observation for

* Corresponding author. Fax: +44 20 7679 7463.
** Corresponding author.
E-mail addresses: L.Cronin@chem.gla.ac.uk (L. Cronin), p.f.mcmillan@ucl.ac.uk (P.F. McMillan).

0022-4596
doi:10.1016/j.jssc.2011.12.005

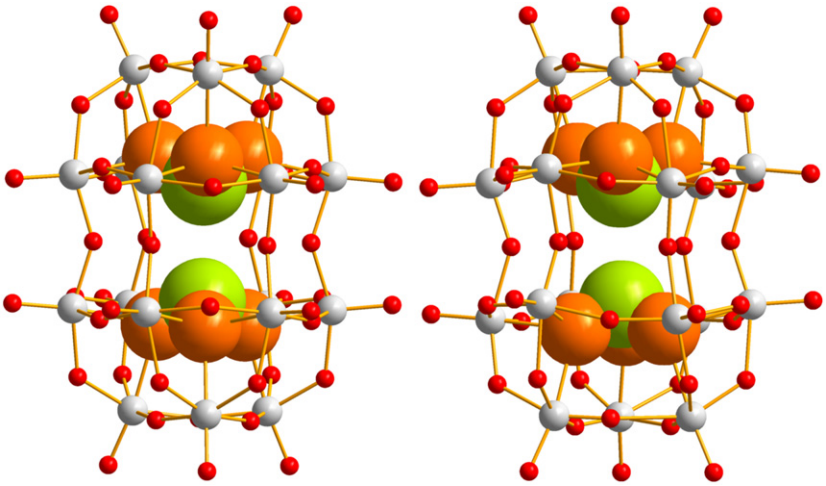

Fig. 1. Representation of the Dawson-like $[Mo_{18}O_{54}(SO_3)_2]^{4-}$ clusters whereby the central sulfite anion templates are shown in a space-filling mode (S: green, O: red, Mo: gray). The oxygen atoms in the SO_3 groups (orange balls) are in eclipsed configuration in the α isomer (left) whereas they are staggered in the β configuration. (For interpretation of the references to color in this figure legend, the reader is referred to the web version of this article.)

POM compounds. Further heating causes disruption of the metal oxide cage. The color changes described and the mechanism and products of the disruption process are studied here by optical, IR and Raman spectroscopy.

The investigation is extended to the behavior and stability of these two structural types at extreme pressure. Similar irreversible color changes were observed upon compression. A comparison is also established between the cluster disruption process occurring either at high temperature or at high pressure. The nature of the products obtained after the cluster collapse at high pressure and the color changes observed will be discussed.

2. Experimental

The synthesis and structural characterization of samples containing $[Mo_{18}O_{54}(SO_3)_2]^{4-}$ polyanions with α or β configurations crystallized using tetrapentylammonium (Pn_4N^+: $Pn=C_5H_{11}$) counter cations were reported previously [7]. Visible spectra were obtained using a home-built instrument based on fiber optics with an Ocean Optics HL-2000 halogen light source and Carl Zeiss MMS1 detector, controlled by Aspect Plus (v1.75) software. FTIR experiments were conducted on powdered samples in KBr disks using a Bruker IFS 66v/S system equipped with a LN2 cooled broadband MCT detector. Micro-Raman experiments were carried out with a Renishaw® system equipped with a CCD detector and diode laser excitation (785 nm), using minimal power levels (<10 mW) to minimize light-induced degradation. High-temperature studies were carried out with a Linkam stage (TS1200) using a $Pt/Pt_{70}Rh_{30}$ thermocouple to measure temperatures. High-pressure studies were conducted using membrane or screw-driven diamond anvil cells (DACs). Type-IIa anvils, 600 μm culet-diameter, were used for optical and FTIR studies. Raman experiments used type-Ia diamonds with 300 μm culet-diameter. Stainless-steel gaskets preindented to 40–50 μm thickness with holes of 150–400 μm drilled by spark-erosion formed the sample chamber. Before loading, samples were precompressed in KBr pellets to reproduce the sample preparation conditions used for the visible and FTIR spectroscopy experiments, then placed in the diamond anvil cell along with cryogenically loaded N_2 as a compression medium. Pressures were determined *in situ* using ruby fluorescence techniques [10].

3. Results and discussion

3.1. High-temperature treatment

The maximum transmission of the α isomer in the visible range occurs at 557 nm followed by a featureless signal rising slightly to longer wavelength, resulting in the yellow color observed at ambient conditions (Fig. 2a). This maximum shifts to 567 nm at ~350 K and the sample becomes orange. This color change is reversible upon recovery to ambient conditions. However, further heating causes an irreversible transformation into a blue phase. At 480 K, the maximum in the transmission spectrum is centered at 465 nm. The visible spectrum of the β isomer at ambient temperature is different. There is a sharp rise in transmission after the 380 nm minimum, followed by a shallower slope to longer wavelength above 550 nm (Fig. 2b). The overall spectrum is featureless in this range and it results in the orange-red color observed at ambient conditions. The slope to longer wavelength increases upon heating to 360 K, resulting in deepening of the red color of the sample. As in the α isomer case, this color change is reversible. Further heating causes an intensity decrease of the slope and a shift of the maximum transmission towards the blue end of the spectrum. The sample is clearly green at 440 K (520 nm) and finally blue at 470 K (490 nm). The latter color changes are irreversible. Selected spectra obtained at intermediate stages during the heating runs are also included in Fig. 2 (dot-dash lines) in order to illustrate the evolution of the spectra associated with the color changes.

The IR spectra of both α- and β-isomers at room temperature (Fig. 3) are dominated by bands at 787, 904 cm^{-1} ($Mo–O_b–Mo$) and 972 cm^{-1} ($Mo=O_t$) from vibrations involving edge-, corner-sharing and terminal oxygen atoms, respectively (Table 1) [11]. The large organic counterions (Pn_4N^+) ensure minimal cluster–cluster interactions so we can consider the $Mo=O_t$ vibration as a pure stretching mode of independent metaloxide cages. The other metal-oxygen vibrations have a combination of stretching and bending character. Vibrational modes from the organic counterions also occur at 1300–1700 cm^{-1} (Fig. 3) and between 2700 and 3000 cm^{-1} (not shown for clarity). The reduction of the clusters was evidenced by the blue color of the samples observed above 430 K, despite the fact that no large variations in the vibrational spectra were observed even up to 460 K. Above this temperature, the intensity of most cluster bands suddenly decreased relative to

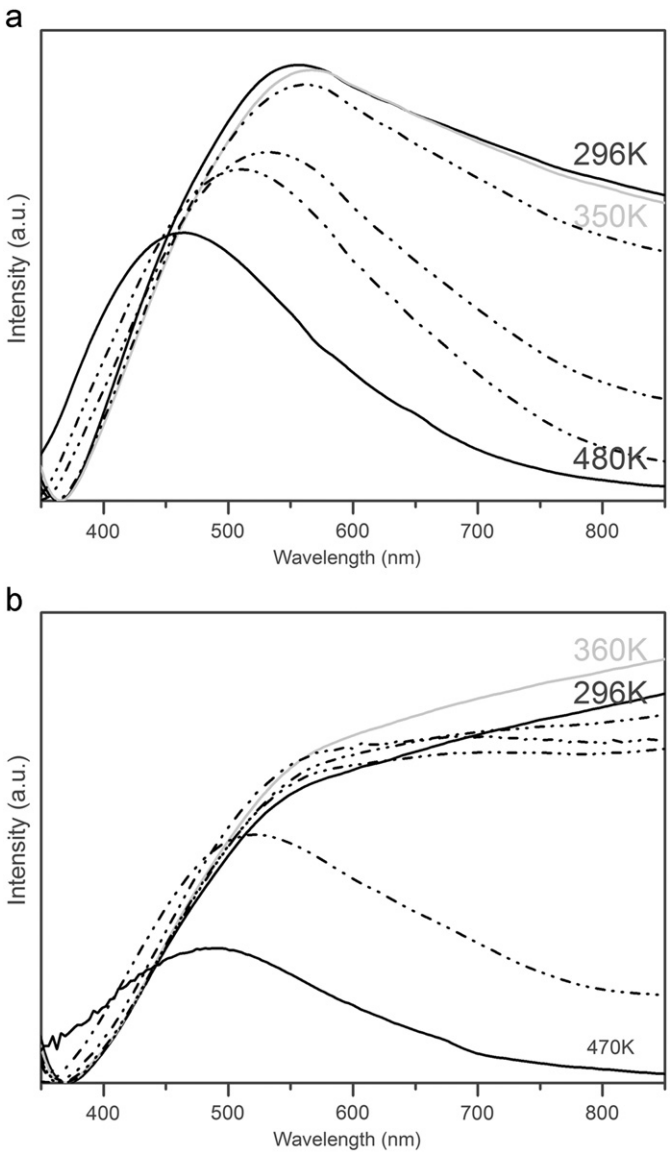

Fig. 2. Transmission spectra of α (a) and β (b) isomers at relevant temperatures. The gray lines represent transmission at the temperature limit of the reversible color change. Further heating causes irreversible color change into green/blue phases. Selected spectra obtained during the heating treatment are included for guidance in the sequence of the color changes (dashed lines).

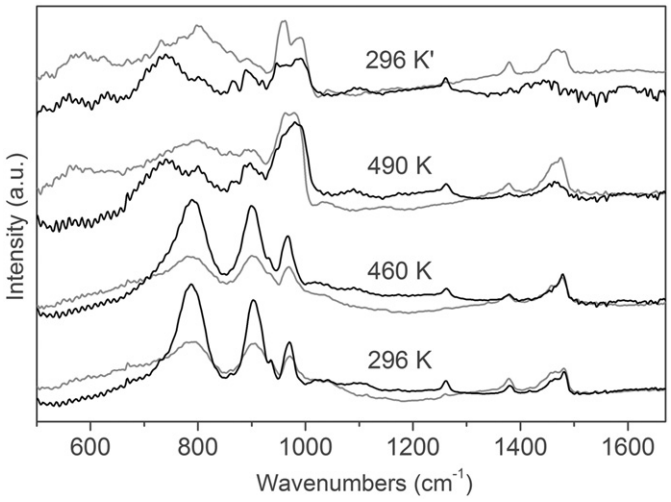

Fig. 3. High-temperature FTIR spectra of α (gray) and β (black) isomers up to 490 K. The recovered spectrum at room temperature is included at the top (296 K).

that of the Mo=O_t mode at $\sim$980 cm^{-1}. The latter mode split into two components, which suggests variations in the O–Mo–O angles that may affect the Mo=O_t bonds. The large changes observed in the Mo–O_b–Mo stretching/bending vibrations between 550 and 900 cm^{-1} indicated the disruption of the clusters at 490 K. The vibrational features in this region indicate that the structures formed from the two cluster types are quite different (Fig. 3). The latter transformations are irreversible, as indicated by the recovered infrared spectrum at ambient conditions (Fig. 3). The IR bands of the organic counter cations (1400–1500 cm^{-1} region) appear to remain unaffected by the thermally induced structural change for the α isomer, but significant changes are observed for the β isomer at 490 K.

The relative intensities of the main infrared bands are plotted in Fig. 4. We note that the Mo=O_t mode (972 cm^{-1}) is relatively insensitive to the changes described at high temperature for both cluster types. It is also important to note that the bands of the α cluster show less relative variation upon heating, suggesting a greater thermal stability of the α isomer. This is consistent with reports that claim a lower Coulombic repulsion and internal strain energy for the α configuration in the case of Keggin ion units [12]. However, the broadening and lower absolute intensity of these bands as compared to those of the β isomer suggest a higher mechanical stability of the latter cluster, considering that both compounds were subjected to similar mechanical treatment including slight grinding to break up the powdered samples followed by pressing into KBr disks for the spectroscopic experiments. Further evidence for the different mechanical stability of both isomers is presented below.

The Raman spectrum of the α and β isomers at ambient conditions is dominated by sharp bands at 992 and 972 cm^{-1}, due to symmetric and asymmetric Mo=O_t vibrations in the clusters (Fig. 5). Bands between 890–850 and 800–760 cm^{-1} are typically assigned to Mo–O–Mo modes involving corner- and edge-sharing oxygen atoms, respectively (Table 1) [11]. Small variations in the positions of these modes occur depending on the isomer configuration. The broad band centered at 618 cm^{-1} is mainly due to O_b–Mo–O_t bending vibrations whereas the strong band at 243 cm^{-1} results from a mixture of symmetric Mo–O_b stretching and Mo–O_b–Mo bending motions. Upon heating to 423 K, the spectrum of the α isomer can only be detected on top of a broad background, and the overall spectrum is considerably weakened. The same effect occurs for the β isomer by 500 K. The deep-blue color of the phases formed at high temperature reduces the penetration depth for the laser within the sample, and the combined effects of thermal and laser-induced degradation must also be taken into account. Our results point to the possible local formation of bronze-like species due to disruption of the clusters at high temperature, that would cause a further reduction in the Raman intensity due to their metallic nature [13,14]. Previous IR studies have reported the synthesis of bronze-like species from Keggin POM precursors [15] or upon reduction of MoO_3 in acidic media [16]. In our case the clusters could open to form sheets of MoO_6 octahedra, retaining the SO_3/SO_4 species within these layers.

3.2. High-pressure treatment

The color changes upon pressurization of the samples were investigated by optical observation (Fig. 6). Both isomers undergo an irreversible piezochromic process from yellow/orange to green upon compression to 18 GPa. A further transformation into a blue

Table 1
IR and Raman frequencies (cm^{-1}) for α and β isomers at room temperature and after transformation at high temperature. Tentative assignments are also included (Ref. 12).

298 K		490 K		Assignment[a]	298 K		490 K		Assignment
IR	Raman	IR	Raman		IR	Raman	IR	Raman	
	84			δ(Mo–O–Mo), δ(O–Mo–O)		625			$\delta(O_b–Mo–O_d)$
	91				787		797		$\nu_{as}(Mo–O_c–Mo)$
	106			δ(Mo–O–Mo), δ(O–Mo–O)		792			$\nu_{as}(Mo–O_c–Mo)$, $\nu_{as}(Mo–O_b)$
	123			δ(Mo–O–Mo), δ(O–Mo–O)		815		820	$\nu_{as}(Mo–O–Mo)$
	139					837			$\nu_{as}(Mo–O_b)$
	155			δ(Mo–O–Mo), δ(O–Mo–O)	860		867		δ(Mo–O–Mo)
	187					863			ν_{as}(Mo–O–Mo)
	203		200		904	895	893		ν_{as}(Mo–O–Mo)
			220/30[a]	δ(Mo–O–Mo)	935				
	234/39[a]			$\nu_s(Mo–O_b)$, $\delta(Mo–O_b–Mo)$	972	969/79[a]	978		$\nu_{as}(Mo–O_t)$
			280	$\nu_{as}(Mo–O_b)$		988		988	$\nu_s(Mo–O_d)$, ν_s(S–O)
	342		350	δ(Mo–O–Mo)	1042		1040		
	381			δ(Mo–O–Mo)	1089		1090		Decomposition product
	410				1150				Decomposition product
	431				1260				
	467			δ(Mo–O–Mo), δ(O–S–O)					

[a] Modes for β isomer are indicated whenever there is a significant difference in the band position of both isomers.

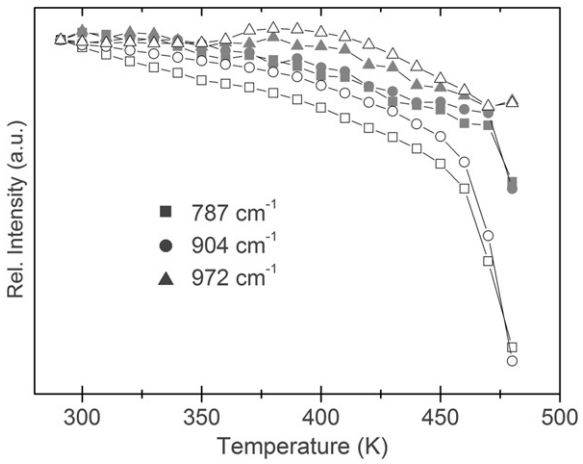

Fig. 4. Normalized relative intensities of the main cluster infrared bands upon heating. Full and empty symbols correspond to α and β isomers, respectively. The bands at 787 and 904 cm^{-1} correspond to $Mo–O_b–Mo$ vibrations involving edge- and corner-sharing oxygen atoms whereas the band at 972 cm^{-1} is from pure $Mo=O_t$ stretching vibrations involving terminal oxygen atoms.

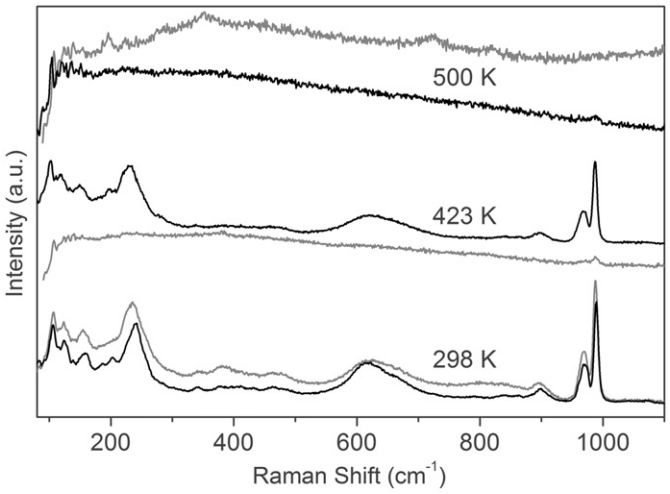

Fig. 5. Raman spectra of α (gray) and β (black) isomers up to 500 K.

phase occurs for the β-isomer, after the sample is held at high pressure for several minutes (Fig. 6).

The main vibrational features from both isomeric clusters are clearly recognizable in the IR spectra obtained in the diamond anvil cell at ambient conditions (Table 1) (Fig. 7). We note that the cluster bands are now comparable in terms of broadening and intensity for both isomers. This reinforces our previous assumption regarding the instability of the α isomer to mechanical treatment, since these samples were not grinded before loading into the KBr pressure transmitting medium during the preparation of the runs at high pressure. The $Mo–O_b–Mo$ mode at 787 cm^{-1} splits into two components immediately after loading into the cell. We can understand this as due to non-hydrostatic stresses that could be developed along with pressure gradients within the sample chamber during initial pressurization. Here the background of the spectra recorded at high pressure contains an interference pattern resulting from multiple IR reflections occurring between the diamond windows, that could not be removed without artificially increasing the spectral broadening. We chose to interpret the peak positions obtained from the raw data as presented. All modes shift to higher wavenumber and broaden upon compression. However, the IR spectra of both isomers show little change up to 8 GPa (Fig. 7). The intensity of all bands decrease upon compression to 18 GPa, including that of the $Mo=O_t$ mode, and there is also substantial band broadening, that indicates the disruption of the clusters, as confirmed by the appearance of the sample spectra after return to ambient conditions (Fig. 7).

The Raman spectrum of the β isomer loaded into the DAC at low pressure (Fig. 8) is comparable with that obtained outside the cell at ambient conditions. However, the spectrum of the α isomer is much weaker, and it contains an additional broad band between 700 and 900 cm^{-1} As pressure increases, this band dominates the spectrum, along with a second broad feature that appears at $\sim$400 cm^{-1} (Fig. 8). A green/blue spot was present in the sample at the point of laser impact after initial runs, indicating that light-induced degradation of the samples could readily take place. Extra care was taken to minimize this effect by reducing the incident laser power to the minimum necessary to observe a Raman spectrum on the experimental timescale, and also selecting a new region within the sample for examination of each spectrum.

The FTIR results at high pressure can be directly compared to those obtained at high temperature, taking into account that the

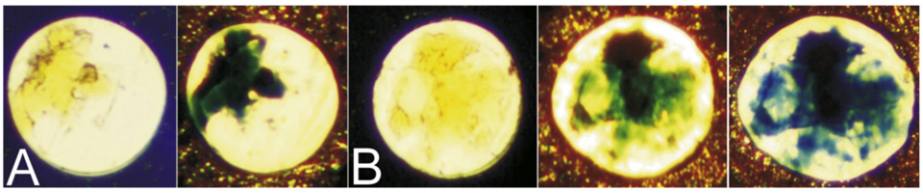

Fig. 6. Microphotographs of α (A) and β (B) isomers loaded in KBr as pressure-transmitting medium in the DAC. The images were taken during an infrared run upon compression. The yellow/orange samples turned green at high pressure. The β isomer changed to blue after being held at high pressure 18 GPa for a few minutes. (For interpretation of the references to color in this figure legend, the reader is referred to the web version of this article.)

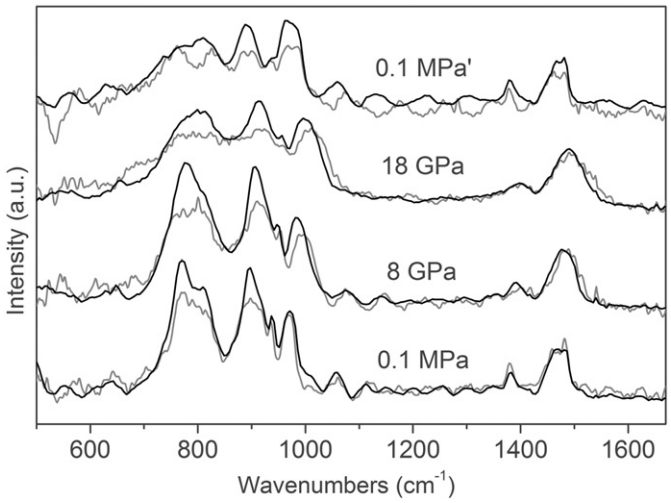

Fig. 7. High-pressure FTIR spectra of α (gray) and β (black) isomers up to 18 GPa. The recovered spectrum is included (0.1 MPa).

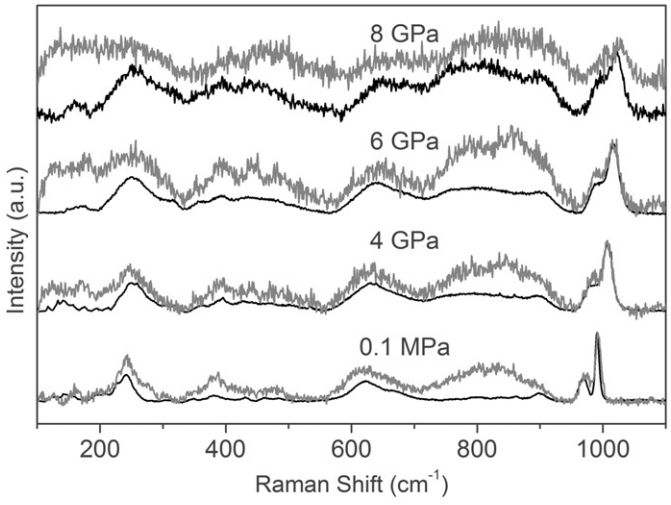

Fig. 8. High-pressure Raman spectra of α (gray) and β (black) isomers up to 8 GPa.

Mo–O_t bonds will be most affected by the increasing density of the material upon pressurization, which explains the decrease in intensity of the corresponding band at 972 cm^{-1}. This observation is consistent with the suggestion that local structures obtained during and following pressurization might become bronze-like in nature. It is relatively easy to envisage opening of the clusters upon heating and the rearrangement of MoO_6 octahedra into MoO_3-like sheets with heterogroups and counterions contained between the layers. However, the structural collapse of clusters at high pressure and low (ambient) T could result in the metastable formation of bronze-like linkages only locally, further kinetically hindered by the presence of large counter-cations and SO_3/SO_4 groups within the cages. The cluster collapse should be favored by the elliptical shape of the Wells–Dawson clusters [17] and it would be accompanied by long-range structural disordering, consistent with the band broadening observed in our IR and Raman data. Broad Raman bands at around 400 and 800 cm^{-1} have been observed to occur during the formation of blue H_xMoO_3 nanobelts from MoO_3, as hydrogen is incorporated in the oxide structure [18]. Our Raman results at high pressure can also be compared with those observed during formation of a bronze-like PW_8O_{26} material via thermal treatment of Keggin POM precursors [15].

Finally, we also note the role of light absorption in the formation of bronze-like materials. The β isomer exhibited a greater resistance to light-induced degradation during the high-pressure Raman experiments. The lower symmetry and higher electronic polarizability of the staggered β configuration may result in a smaller HOMO–LUMO gap, which favors greater orbital mixing and thus greater stability of this isomer [19]. A higher repulsion between the internal oxygen atoms in the eclipsed configuration is also expected upon increasing density, which contributes to the instability of the α isomer at high pressure.

4. Conclusions

The stability of large sulfite-based Wells–Dawson α/β-$[Mo_{18}O_{54}(SO_3)_2]^{4-}$ clusters was explored under extreme pressure and temperature conditions. The staggered β configuration of internal oxygen atoms showed greater stability under mechanical processing, whereas the eclipsed α configuration was more stable upon heating. The latter cluster was more susceptible to light-induced degradation, however.

Spectroscopic evidence has been presented for the formation of locally bronze-like species from non-conventional POM compounds above 400 K and also at ~8 GPa. The different nature of the bronze-like species produced by high-temperature and high-pressure conditions results from cluster opening during heating vs collapse at high pressure. These studies reveal the potential of high pressure vs high temperature studies as a tool to study and prepare different nanoscale bronze-like materials, and laser-induced local degradation of the highly light-sensitive POMs could also be exploited.

Acknowledgments

The contributions of PFM and RQC were supported by EPSRC Senior Research Fellowship D07357X to PFM. LC thanks the Wolfson Foundation/Royal Society for a research merit award.

References

[1] D.-L. Long, E. Burkholder, L. Cronin, Chem. Soc. Rev. 36 (2007) 105–121.
[2] A. Bither, J.L. Gillson, H.S. Yong, Inorg. Chem. 5 (1966) 1559–1562.

[3] V.V. Lisnyak, N.V. Stus, D.A. Stratiychuk, V.M. Tkach, P. Popovich, J. Alloy Compd. 359 (2003) 307–309.
[4] A. Anzai, K. Inumaru, S. Yamanaka, J. Alloy. Compd. 470 (2009) 557–560.
[5] R. Quesada Cabrera, D.-L. Long, L. Cronin, P.F. McMillan, CrystEngCommun. 12 (2010) 2568–2572.
[6] D.-L. Long, P. Kögerler, L. Cronin, Angew. Chem. Int. Ed. 43 (2004) 1817–1820.
[7] C. Baffert, J.F. Boas, A.M. Bond, P. Kögerler, D.-L. Long, J.R. Pilbrow, L. Cronin, Chem. Eur. J. 12 (2006) 8472–8483.
[8] R. Tsunashima, D.-L. Long, T. Endo, S-I. Noro, T. Akutagawa, T. Nakamura, P. Kögerler, R. Quesada Cabrera, P.F. McMillan, L. Cronin, Phys. Chem. Chem. Phys. 13 (2011) 7295–7297.
[9] C. Fleming, D.-L. Long, N. McMillan, J. Johnston, N. Bovet, V. Dhanak, N. Gadegaard, P. Kögerler, L. Cronin, M. Kadodwala, Nat. Nanotechnol. 3 (2008) 229–233.
[10] R.A. Forman, G.J. Piermarini, J.D. Barnett, S. Block, Science 176 (1972) 284–285.
[11] C. Rocchiccioli-Deltcheff, R. Thouvenot, M. Fouassier, Inorg. Chem. 21 (1982) 30–35;
C. Rocchiccioli-Deltcheff, M. Fournier, R. Franck, R. Thouvenot, Inorg. Chem. 22 (1983) 207–216;
R. Thouvenot, M. Fournier, R. Franck, C. Rocchiccioli-Deltcheff, Inorg. Chem. 23 (1984) 598–605.
[12] R.I. Buckley, R.J.H. Clark, Coord. Chem. Rev. 65 (1985) 167–218;
D.L. Kepert, Inorg. Chem. 8 (1969) 1556–1558.
[13] S. Nishio, M. Kakihana, Phys. Rev. B 63 (2001) 033104-1–033104-4;
T. Hirata, K. Ishioka, M. Kitajima, Appl. Phys. Lett. 68 (1996) 458–460.
[14] K. Wassermann, M.T. Pope, M. Salmen, J.N. Dann, H-J. Lunk, J. Solid State Chem. 149 (2000) 378–383;
H. Weiner, H-J. Lunk, B. Ziemer, K. Köhnke, C. Pietzsch, Thermochim. Acta 244 (1994) 93–103;
P.G. Dickens, A.C. Halliwell, D.J. Murphy, M.S. Whittingham, Trans. Faraday Soc. 67 (1971) 794–800.
[15] U.B. Mioc, R.Z. Dimitrijevic, M. Davidovic, Z.P. Nedic, M.M. Mitrovic, PH. Colomban, J. Mater. Sci. 29 (1994) 3705–3718.
[16] N. Sotani, K. Eda, M. Sadamatu, S. Takagi, Bull. Chem. Soc. Jpn. 62 (1989) 903–907.
[17] S. Shikata, S. Nakata, T. Okuhara, M. Misono, J. Catal. 166 (1997) 263–271.
[18] X.K. Hu, Y.T. Qian, Z.T. Song, J.R. Huang, R. Cao, J.Q. Xiao, Chem. Mater. 20 (2008) 1527–1533.
[19] Y.-R. Guo, Q.-J. Pan, Y.-D. Wei, Z.-H. Li, X. Li, J. Mol. Struct. (Theochem.) 676 (2004) 55–64.